*International Refereed Journal of Engineering and Science (IRJES)*
*ISSN (Online) 2319-183X, (Print) 2319-1821*
*Volume 2, Issue 7 (July 2013), PP. 38-43*
*www.irjes.com*

# An Initial Assessment of a Perimetric Function Added To A Fundus Camera to Create Optic Nerve Fibre Maps

N. Suzuki
*(Department of Medical Science and Technology, Hiroshima International University, Japan)*

***ABSTRACT:-*** *Diabetic retinopathy and glaucoma are the main causes of blindness in the elderly. Here we report an experimental device that we constructed using the same optical system as found in a fundus camera, and investigated various methods to diagnose diabetic retinopathy. Glaucoma causes damages to the optic nerve fibres. Arcuate scotoma and nasal steps comprise a series of scotomata along the optic nerve fibres in glaucoma patients. We generated an optic nerve fibre map using the perimetric function of our experimental device. Photographs of the fundus were captured to determine the locations of the fovea centralis and optic disc before the examination. An optic nerve fibre map was generated using Borland C++ Builder v5.0 software and superimposed on the fundal image. The software was used to calculate the location of the examination target along the direction of the retinal nerve fibres.*

***Keywords:-*** *Fundus Camera, Perimeter, Optic nerve fibre map and Glaucoma*

## I. INTRODUCTION

Diabetic retinopathy and glaucoma are the main causes of blindness in the elderly. According to a study conducted in 1999 in the United States, the number of diabetics was estimated to increase from 16 to 30 million over the next 30 years [1]. In comparison, there were 16.2 million confirmed and potential diabetics in Japan in 2005 [2]. Here we constructed an experimental device using the same optical system found in a fundus camera and investigated various methods to distinguish small retinal haemorrhages caused by diabetic retinopathy from dust artefacts using the hue, lightness and saturation (HLS) colour system [3]. In the HLS colour space, lightness and saturation enabled the distinction of haemorrhages from dust artefacts under almost all conditions.

In contrast, more than 4 million Americans have glaucoma [4] and an estimated 70 million are suspected of having the disease worldwide [5]. Glaucoma is discovered by inspecting abnormalities in a visual field, as the disease causes gradual obstruction of the optic nerve resulting in narrowing of the visual field. Patients with early stages of glaucoma rarely notice symptoms; therefore, examinations of a patient's visual field should be performed periodically for glaucomatous advances.

We added a perimetric function to our experimental device using the same optical system as found in a fundus camera to generate a unique optic nerve fibre map for each patient. The optic nerve fibres are different in all individuals. Because it is very difficult to assess optic nerve fibres without injury, we gave precedence to the whole system over just measurements of the optic nerve fibres.

Glaucoma causes the following disorders in optic nerve fibres. Optic nerve fibre bundles travel towards the optic disc from all sites in the retina [6], [7]. When a disorder occurs in the nerve pathway, optic nerve fibre bundles entering the upper and lower poles of the optic disc are the first to be impaired, as in typical glaucoma, which leads to visual field defects [8]. When optic nerve fibre bundles are impaired in the optic disc, the visual field region governed by these fibres loses function, leading to scotoma and local depression. Consequently, isolated paracentral scotoma or arcuate scotoma with multiple scotomata fused together, appear in the Bjerrum area: the nasal visual field is impaired, or both the scotomata occur simultaneously. Arcuate scotoma occurrence is caused by greater impairment of the optic nerve fibre bundles than isolated scotoma. Defects in the optic nerve fibre bundles begin in the optic disc detour in an arc around the fixation point, and results in scotoma extending to the nasal horizontal meridian. Glaucomatous changes in the optic disc have been reported to be a cause of nerve fibre layer defects [9] – [13]. In addition, glaucoma is frequently associated with different degrees of impairment of the upper pole of the optic disc and corresponding impairment of the lower pole. The difference is particularly large when a comparison is made between directly above and below the nasal horizontal meridian in a visual field diagram. This is because, on the temporal side of the retina, the optic nerve fibre bundles directly above the horizontal meridian travels the upper half of the optic disc, while the fibres directly below travels the lower half. This inconsistency above and below the nasal horizontal meridian has been clarified by kinetic perimetry, in which the examination target is moved along the horizontal meridian. Since the upper and lower isopters differ, a nasal step results as described by Bjerrum and Roenne [14].

Nasal step is detected as a difference in the light sensitivity threshold bordering the horizontal meridian of the nasal visual field. This change in the visual field corresponds to impairment of one of the upper and lower optic nerve fibre bundles. Impairment of the optic nerve fibre bundles in which nasal step occurs is present at sites closer to the upper and lower poles of the optic disc than in the case of isolated scotoma. Kinetic perimetry demonstrates invagination to the inside of the isopter on the nasal side. Even when there is no local impairment of the optic disc, retinal nerve fibres are locally impaired on the supratemporal or subtemporal sides. Glaucomatous impairment is frequently localized over an extremely narrow range, and regions with extension exhibit abnormalities causing decreased sensitivity. Although partial overlapping occurs following repeated testing, abnormalities are observed in different regions [15] – [20].

Thus, the loci of the optic nerve fibre relate to glaucoma very well, but photographs of the loci of the optic nerve fibre bundles are difficult to obtain without causing injury. When taking a photograph of the fundus using a fundus camera or a scanning laser ophthalmoscope, little can be seen off the optic nerve fibre bundles. We have generated an optic nerve fibre map based on a sketch in an atlas [21].

## II. METHODS

### 1. Making the nerve fibre map

We made a retinal nerve fibre map, as shown in Fig.1. The center position of the optic disc is at temporal longitude. The map has 22 curves (S-1-11 and I-1-11) and four horizontal lines (S-0, S-12, I-0 and I-12). The vertical range is －25° to 25° latitude. The horizontal range is －16° to 25° longitude. Each curve on the superior field almost contrasts with each curve on the inferior field. Sixteen curves (S-1-7, S-11, I-1-7 and I-11) and four lines (S-0, S-12, I-0 and I-12) are plotted per 0.667° ( 2 / 3° ) longitude. Six curves (S-8-10 and I-8-10) are plotted per 0.667° ( 2 / 3° ) latitude. The right-hand part of Fig.1 shows the relationship of each curve to the optic disc. $\theta_s$ And $\theta_i$ are the angles between the horizontal line and a line at 15° longitude to the rim of the optic disc.

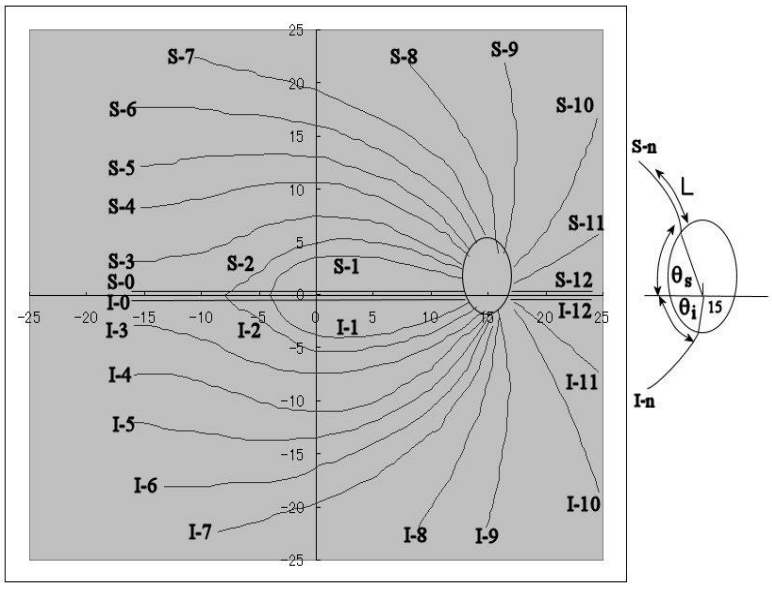


**Fig.1** Retinal nerve fibre map

**Table 1:** Angle ( $\theta_s$ , $\theta_i$ ) between the horizontal line and a line at 15° longitude to the rim of the optic disc.

| SI- | 0 | 1 | 2 | 3 | 4 | 5 | 6 | 7 | 8 | 9 | 10 | 11 | 12 |
|---|---|---|---|---|---|---|---|---|---|---|---|---|---|
| $\theta_s$ ° | 0 | 35 | 45 | 55 | 65 | 75 | 80 | 90 | 100 | 110 | 130 | 155 | 180 |
| $\theta_i$ ° | 0 | 25 | 50 | 70 | 80 | 90 | 100 | 115 | 120 | 130 | 155 | 165 | 180 |

### 2. Optic nerve fibre map superimposed on the fundus image

To align the examination target in the loci of the optic nerve fibre bundles for static visual field examination, photograph of the fundus was taken prior to the examination to determine the locations of the fovea centralis and optic disc. In Fig.2, the optic nerve fibre map was enlarged or reduced to superimpose the fovea centralis of the fundus image with the disc.

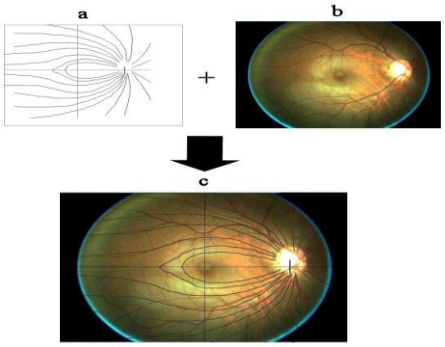


**Fig.2** Fundus photograph and optic nerve fibre bundle template.
Optical nerve fibre map (a), fundus photograph (b) and optical nerve fibre map on a fundus photograph (c).

The size of the optic disc varies even among healthy individuals, ranging from an eightfold opening to a small cup in individuals with smaller optic discs. There are individuals with large optic disc, in which the C/D ratio exceeds 0.7 despite the absence of glaucoma. Consequently, the center of the disc is used as a reference for aligning the fundus photograph and disc location of the map.

Examinations were performed using the loci of 26 optic nerve fibre bundles extracted at visually equal intervals from the infinite number of optic nerve fibre bundles and then moving the examination target along a new curve determined by equation (1).

Fig.3 indicates a method for calculating the loci of retinal nerve fibre bundles. Point O indicates the fovea centralis. The X-axis is taken from point O in the horizontal direction, while the Y-axis is taken from point O in the vertical direction. The oval on the right edge indicates the optic disc. The dotted line curve from the optic disc indicates nerve fibres. The hatched area indicates the diseased area. A certain point P ( $x_p$, $y_p$ ) in the diseased area is selected. The points that intersect with nerve fibres in the vertical direction from point P are represented by $Q_u$ ( $x_{qu}$,$y_{qu}$ ) and $Q_d$ ( $x_{qd}$, $y_{qd}$).

A new curve is then determined with the same ratio as equation (1).

$$\left|y_{qu}-y_p\right| : \left|y_p-y_{qd}\right| \qquad (1)$$

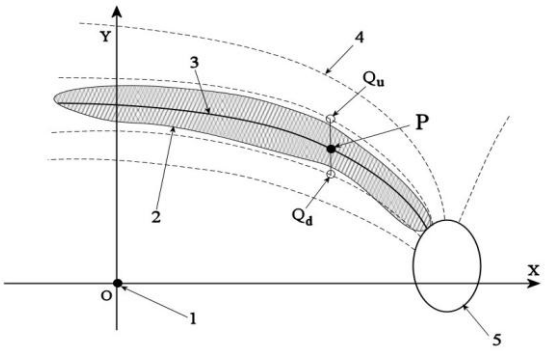


**Fig.3** Method for calculating the direction of orientation of retinal nerve fibres.
Fovea centralis (1), diseased area (2), new curve (3), nerve fibre (4) and optic disc (5).

This optic nerve fiber map was created using VAIO PCG-7U1N computer (Sony Corporation, Tokyo, Japan) with Borland C++ Builder 5.0 software.

### 3. Experimental device

We constructed an experimental device using the same optical system found in a fundus camera [22]. As shown in Fig.4, the experimental device is equipped with an illumination optical system and a photographic optical system that are separated by a mirror containing a hole with a 4-mm diameter. The device consists of a canon EOS 50D camera, an EF 50 mm f/1.8-2 camera lens, a Speedlite 270EX flash, an object lens with a focal length of 50 mm, four double-convex lenses with focal lengths of 100 mm, three aperture stops, a mirror and an artificial eye.

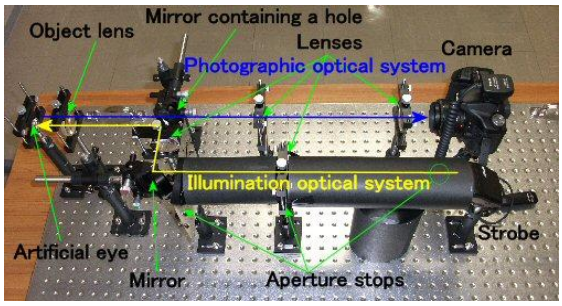


**Fig.4** Experimental device

As shown in Fig.5, we substituted an infrared camera for the colour camera and a halogen lamp for the strobe light source in our experimental device. Furthermore, we added an optical system that was equipped with both a display and a half mirror. The visual field test shows an examination target on the display.

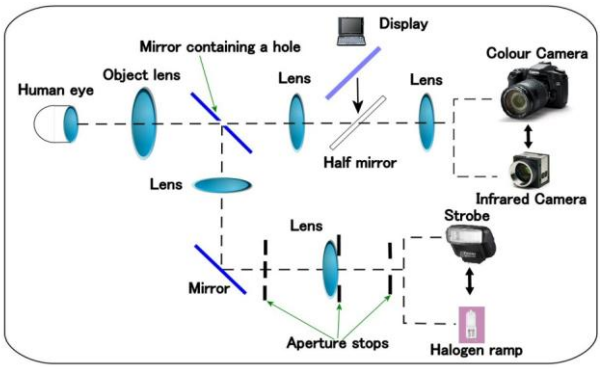


**Fig.5** Addition of a perimetric function to the experimental device

## III. RESULTS

### 1. Optic nerve fibre map superimposed on the fundus image

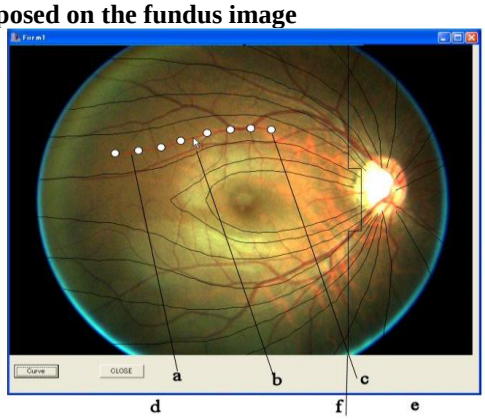


Fig.6 How to calculate a new curve.
New curve (a), mouse (b), examination targets (c), vertical area (d), horizontal area (e).

Fig.6 is an illustration of the software used to calculate the location of the examination target along the direction of the retinal nerve fibres. A new curve is determined according to the method shown in Fig.3, and the locations of examination targets are then determined on that curve. Determination of these targets makes it possible to show examination targets on the display of the experimental device. Fig.6 (f) indicates the boundary between the vertical area and the horizontal area. In the vertical area, the new curve is determined according to the method shown in Fig.4.

## IV. DISCUSSION

### 1. Optic nerve fibre map

We used an atlas to generate the map because it is difficult to take a photograph of the optic nerve fibre bundles without causing injury. The map has 22 curves and 4 horizontal lines (S-0, S-12, I-0 and I-12). Each

curve on the superior field almost corresponds with the respective curve on the inferior field. All the nerve fibre lines have a relationship with the angle $\theta_s$ or $\theta_i$.

**2. New curve**

A new curve was calculated that passes through a point clicked on by the mouse on the fundus image. This calculation uses the ratio between the distances from two neighbouring curves. We can use a map that has more than 26 lines if there are problems with the ratio between the two distances.

**3. Future work**

Polarization-sensitive Fourier domain optical coherence tomography (PS-FD-OCT) is one of the techniques in measuring the optic nerve fibres. In the future work, we will adopt PS-FD-OCT to this system. This PS-FD-OCT applied the circularly polarized light [23] – [26], Stokes' vector [27] – [30], Mueller matrix [31] ,[32] and Jones matrix [33] – [38].

## V. CONCLUSION

We generated an optic nerve fibre map using the perimetric function of our experimental device. The optic nerve fibre map was generated using Borland C++ Builder v5.0 software and superimposed on the fundal image. The software was used to calculate the location of the examination target along the direction of the retinal nerve fibres.

## VI. ACKNOWLEDGEMENTS

For research expenses, the intramural budget of Hiroshima International University was used. We are very thankful to all those who helped in our research.

## REFERENCES

[1] Z.T. Bloomgarden, American Diabetes Association Annual Meeting, 1999, Diabetes and obesity, *Diabetes Care 23(1)*, 2000, 118-124
[2] T. Tsuchiya, Measure Against Lifestyle Related Disease, *JMAJ 49(3)*, 2006, 132-134
[3] N. Suzuki, Research on a method for distinguishing small retinal haemorrhages from dust artefacts using HLS colour space, *International Referred Journal of Engineering and Science 1(4)*, 2012, 13-22
[4] Prevent Blindness America.
[5] H.A. Quigley, Number of people with glaucoma worldwide, *British Journal of Ophthalmology 80(5)*, 1996, 389-393
[6] F. Vrabec, The temporal raphe of the human retina, *Am J Ophthalmol 62*, 1966, 926-938
[7] T. Sakai, K. Sano, K. Tsuzuki, M. Ueno, Y. Kawamura, Temporal raphe of the retinal fiber layer revealed by medullated fibers, *Jpn J Ophthalmol 31*, 1987, 655-658
[8] W.F. Hoyt, L. Frisen, N.M. Newman, Fundoscopy of nerve fiber layer defect in glaucoma, *Invest Ophthalmol 12*, 1973, 814-829
[9] H.A. Quigley, W.R. Green, The histology of human glaucoma cupping and optic nerve damage, *Ophthalmology 86*, 1979, 1803-1830
[10] H.A. Quigley, E.M. Addicks, W.R. Green, A.E. Maumenee, Optic nerve damage in human glaucoma Ⅱ, *Arch Ophthalmol 99*, 1981, 635-649
[11] H.A. Quigley, E.M. Addicks, W.R. Green, Optic nerve damage in human glaucoma Ⅲ. *Arch. Ophthalmol 100*, 1982, 135-146
[12] H.A. Quigley, E.M. Addicks, Regional differences in the structure of lamina cribrosa and their relationship to glaucomatous optic nerve damage, *Arch. Ophthalmol 99*, 1981, 137-143.
[13] H.A. Quigley, E.M. Addicks, Quantitative studies of retinal nerve fiber defects, *Arch. Ophthalmol 100*, 1982, 807-814
[14] H. Ronne, Uber das Gesichtfeld beim Glaulsom, *klin Monastsbl Augenheilkd 47*, 1909, 12-33
[15] J. Flammer, S.M. Drance, M. Zulauf, Differential light threshold:Short-and-long-term fluctuation in patients with glaucoma, normal controls, and patients with suspected glaucoma, *Arch Ophthalmol 102*, 1984, 704-706
[16] A. Heijl, G. Lindgren, J. Olsson, P. Asman, Visual field interpretation with empiric probability maps, *Arch Ophthalmol 107*, 1989, 204-208
[17] C. Holmin, C.E. Krakau, Variability of glaucomatous visual defects in computerized perimetry, *Albrecht Von Arch Klin Exp Ophthalmol 210*, 1979, 235-250.
[18] E.B. Werner, S.M. Drance, Early visual field disturbances in glaucoma, *Arch Ophthalmol 95*, 1977, 1173-1175
[19] E.B. Werner, S.M. Drance, Increased scatter of responses as a precursor of visual field changes in glaucoma, *Can J Ophthalmol 12*, 1977, 140-142
[20] E.B. Werner, N. Soheb, D. Thomas, Variability of static visual threshold responses in patients with elevated IOPs, *Arch Ophthalmol 100*, 1982, 1627-1631
[21] J.A. Alvarado, Histlogy of the Human Eye. An atlas and the textbook, Saunders, Philadelphia, 1971.
[22] N. Suzuki, Research on a method for distinguishing small retinal haemorrhages from dust artefacts using HLS colour space, *International Referred Journal of Engineering and Science 1(4)*, 2012, 13-22

[23] M.R. Hee, D. Huang, E.A. Swanson, J.G. Fujimoto, Polarization-sensitive low-coherence reflectometer for birefrigence characterization and ranging, *J. Opt. Soc. Am. B9*, 1992, 903-908
[24] J.F. de Bore, T.E. Milner, M.J.C. van Gemert, J.S. Nelson, Two-dimensional birefringence imaging in biological tissue by polarization-sensitive optical coherence tomography, *Opt. Lett. 22*, 1997, 934-936
[25] C.K. Hitzenberger, E. Gotzinger, M. Sticker, M. Pircher, A.F. Fercher, Measurement and imaging of birefringence and optic axis orientation by phase resolved polarization sensitive optical coherence tomography, *Opt. Express 9*, 2001, 780-790
[26] E. Gotzinger, M. Pircher, C.K. Hitzenberger, High speed spectral domain polarization sensitive optical coherence tomography of the human retina, *Opt. Express 13*, 2005, 10217-10229
[27] J.F. De Boer, T.E. Milner, J.S. Nelson, Determination of the depth-resolved Stokes parameters of light backscattered from turbid media by use of polarization-sensitive optical coherence tomography, *Opt. Lett. 24*, 1999, 300-302
[28] C.E. Saxer, J.F. de Bore, B.H. Park, Y. Zhao, Z. Chen, J.S. Nelson, High-speed fiber-based polarization-sensitive optical coherence tomography of in vivo human skin, *Opt. Lett. 25*, 2000, 1355-1357.
[29] J. Zhang, W. Jung, J.J. Nelson, Z. Chen, Full range polarization- sensitive Fourier domain optical coherence tomography, *Opt. Express 12*, 2004, 6033-6039
[30] B. Cense, T.C. Chen, M. Mujat, C. Joo, T. Akkin, B.H. Park, M.C. Pierce, A. Yun, B.E. Bouma, G.J. Tearney, J.F. de Boer, Spectral-domain polarization-sensitive optical coherence tomography at 850 nm, *Proc. of SPIE 5690*, 2005, 159-162
[31] G. Yao, L.V. Wang, Two-dimensional depth-resolved Mueller matrix characterization of biological tissue by optical coherence tomography, *Opt. Lett.24*, 1999, 537-539
[32] Y. Yasuno, S. Makita, Y. Sutoh, M. Itoh, T. Yatagai, Birefrigence imaging of human skin by polarization-sensitive spectral interferometric optical coherence tomography, *Opt. Lett. 27*, 2002, 1803-1805
[33] S. Jiao, L.V. Wang, Two-dimensional depth- resolved Mueller matrix of biological tissue measured with double-beam polarization-sensitive optical coherence tomography, *Opt. Lett. 27*, 2002, 101-103
[34] S. Jiao, W. Yu, G. Stoica, L.V. Wang, Optical-fiber-based Mueller optical coherence tomography, *Opt. Lett. 28*, 2003, 1206-1208
[35] B.H. Park, M.C. Pierce, B. Cense, J.F. de Boer, Jones matrix analysis for a polarization-sensitive optical coherence tomography system using fiber-optic components, *Opt. Lett. 29*, 2004, 2512-2514
[36] B.H. Park, M.C. Pierce, B. Cense, S.H. Yun, M. Mujat, G.J. Tearney, B.E. Bouma, J.F. de Boer, Real-time fiber-based multi-functional spectral-domain optical coherence tomography at 1.3 μm, *Opt. Express 13*, 2005, 3931-3944
[37] S. Jiao, M. Todorovic, G. Stoica, L.V. Wang et al, Fiber-based polarization-sensitive Mueller matrix optical coherence tomography with continuous source polarization modulation, *Appl. Opt. 44*, 2005, 5463-5467
[38] Y. Yasuno, S. Makita, T. Endo, M. Itoh, T. Yatagai, M. Takahashi, C. Katada, M. Mutoh, Polarization-sensitive complex Fourier domain optical coherence tomography for Jones matrix imaging of biological samples, *Appl. Phys. Lett 85*, 2004, 3023-3025.